



#### Available online at www.sciencedirect.com

## **ScienceDirect**

Advances in Space Research 76 (2025) 2561-2577

ADVANCES IN SPACE RESEARCH
(a COSPAR publication)

www.elsevier.com/locate/asr

# Evaluation of CryoSat-2 ocean products through routine monitoring and a 13-year long consistent time series dataset

Christopher J. Banks <sup>a,\*</sup>, Francisco Mir Calafat <sup>a,b</sup>, Alessandro Di Bella <sup>c</sup>

<sup>a</sup> National Oceanography Centre, Joseph Proudman Building, 6 Brownlow Street, Liverpool L3 5DA, United Kingdom

<sup>b</sup> Department of Physics, University of the Balearic Islands, Carretera de Valldemossa, km 7,5, 07122 Palma, Balearic Islands, Spain

<sup>c</sup> EOP-GMQ, Sensor Performances, Products and Algorithms Office, Earth Observation Ground Segment Department, ESRIN, Largo Galileo Galilei 1, 00044 Frascati, Italy

Received 24 January 2025; received in revised form 17 June 2025; accepted 19 June 2025 Available online 23 June 2025

#### **Abstract**

CryoSat-2 (C2) was launched in 2010 and has been retrieving values of sea surface height anomaly (SSHA), significant wave height (SWH) and wind speed (WSP) ever since. Although these oceanographic variables were secondary aims, an operational CryoSat Ocean Processor was implemented in 2014. This study provides details on the routine monitoring process for the various products alongside additional analyses using a 13-year dataset of quality-controlled Baseline C data. Most of this study focussed on Low Resolution Mode (LRM) data with some specific studies of Synthetic Aperture Radar (SAR) mode. No substantial issues with the data were observed but additional studies of SWH and WSP are recommended.

Global mean sea level (GMSL) from C2 has a trend of  $4.2 \pm 0.3$  mm/year which agrees, within uncertainties, from other data sources. Regionally the patterns in SSHA trend agree with other sources. SWH from similar analyses found no significant trend but WSP trend was  $3.3 \pm 0.2$  (cm/s)/year. For GMSL and WSP data from descending passes (C2 moving south) have non-significantly higher trends compared to data from ascending passes. Regionally, apart from a few, small areas (primarily around Southeast Asia), trends in C2 WSP are positive and agree with a previous study using multiple altimeters.

Biases have been identified including between LRM and SAR using successive differences in SSHA, SWH and WSP. Similarly, seasonally varying biases between ascending passes and descending passes are found, which in turn vary by hemisphere.

Comparisons were made between tide gauges based on data from the Permanent Service for Mean Sea Level (PSMSL) and gridded (1°) SSHA from C2. For both LRM and SAR, the significant correlations were positive and similar, albeit slightly lower, to previous studies.

Routine reports compare C2 SWH to that from the WaveWatch3 model (WW3) with the latter on average (mean) ~15 cm higher with a few exceptions. This was confirmed using WW3 and C2 SWH on the same monthly grid where the difference was found to be 10–20 cm, and all correlations were positive (~0.8–0.9). There are strong differences between C2 SWH and WW3 by hemisphere (bias is greater in Southern Hemisphere) and the variability of correlations is greater in the Northern Hemisphere. The relationship is more complex as there is some evidence that at low SWH WW3 tends to be higher than C2 whereas at higher SWH C2 SWH is higher than WW3.

There is a bias between C2 WSP and that from ERA5 that is negative (ERA5 WSP higher than C2 WSP) at higher WSP and a less pronounced positive bias at low WSP. Comparisons of trends in WSP from C2 compared to ERA5 are more complex and patterns in both do not fully match. These results are possibly as a result of altimeters being unable to resolve low WSP (<~2 m/s).

© 2025 The Author(s). Published by Elsevier B.V. on behalf of COSPAR. This is an open access article under the CC BY license (http://creativecommons.org/licenses/by/4.0/).

Keywords: Satellite altimetry; Significant wave height; Ocean wind speed; Global mean sea level; Sea surface height; CryoSat

E-mail addresses: Chris, Banks@noc.ac.uk (C.J. Banks), Francisco.MCalafat@uib.es (F.M. Calafat), Alessandro.DiBella@esa.int (A. Di Bella).

<sup>\*</sup> Corresponding author.

#### 1. Introduction

CryoSat-2 (C2) was the first European ice mission launched by the European Space Agency in 2010. C2's Synthetic Aperture Interferometric Radar Altimeter (SIRAL) was primarily designed for measuring sea ice freeboard and ice sheets. However, the use of SIRAL data over global oceans was a secondary requirement, and operational ocean products were developed from 2014 onwards via the CryoSat Ocean Processor (COP).

The COP provides a number of data products (Time Critical/TC: Near real time Ocean Product, NOP; Interim Ocean Products, IOP; and Non-time Critical/NTC Geophysical Ocean Products, GOP). NOP are typically available within three hours of acquisition and IOP within three days. GOP are available within about 30 days of acquisition and use consolidated orbits and as such represent the best quality of the three data products.

Section 2 of this paper provides an introduction to the routine quality control (QC) routines performed by the National Oceanography Centre (NOC). The NOC provides routine daily and monthly reports on COP products and these are readily available from https://qras.earth.esa.int/?mis=CryoSat&ins=SIRAL.

Section 3 introduces the additional analyses of this study using a 13-year dataset of quality-controlled GOP data. Specifically, we present results of the current operational processing version (Baseline C), which was introduced in late 2017 in Section 4. A new processor version (Baseline D) was introduced in October 2024 and as such this paper, in association with the reports introduced in the next section, can be considered as a final summary of the quality of Baseline C ocean data. Readers interested in the performance of Baseline D can consult the reports presented in Section 2 below.

For dates before November 2017 the data presented are the reprocessed data whereas later data were produced by the operational processing chain. We report on the quality of significant wave height (SWH) and wind speed (WSP) as available in the GOP data and a value of sea surface height anomaly (SSHA) calculated from variables within the data files. Similar analyses from the earlier Baseline B data can be found in the routine reports (using the above URL) as well as, for example, in Bouffard et al. (2018), Calafat et al. (2017), or Naeije and Bouffard (2021).

C2 operates in a variety of modes over the ocean, this is primarily Low Resolution Mode (LRM; conventional pulse limited altimeter). Many coastal regions are covered in Synthetic Aperture Radar (SAR; enhanced along-track resolution also known as Delay Doppler Altimetry) mode. The other mode is Synthetic Aperture Radar Interferometric (SARIn) and is primarily used over ice sheet edges where SAR is enhanced by the use of a second antenna (Parrinello et al., 2018) which enables the relocation of the echoes in the across-track direction. LRM is of sufficient resolution for most oceanographic purposes with the notable exception of coastal and polar regions. In

coastal regions SAR has proved to be of significant benefit in both lowering noise and measuring closer to the shore (Benveniste et al., 2019; Vignudelli et al., 2019; Fenoglio et al., 2021) as has specialised retracking of LRM data (e.g. Passaro et al., 2014; Cazenave et al., 2022). The operating mode over any given location can be varied and is predefined using the mode mask and an example of this is given in Fig. 1.

It is worth noting that unlike most satellite altimeters, until 2020 C2 had a long repeat orbit (~369 days with a 30-day sub-cycle) chosen to provide a high number of cross-over points in polar regions as well as covering southern Greenland (Bouffard et al., 2018). Since 2020, the orbit of C2 was changed with the beginning of the CRYO2ICE campaign to provide near-coincident measurement with NASA's ICESat mission.

Naeije et al. (2023) have recently identified a number of issues with the quality of the SIRAL data including issues with the corrections for the ionosphere and pole tide; a *jump* in significant wave height between SAR and LRM; and a bias in range between ascending and descending passes.

In the next section, we present sample results from the routine quality control reports along with details of the QC philtres applied to data in these reports and the longer time series GOP data in Sections 3 and 4.

#### 2. Routine quality reports and quality control

A standard approach to QC has been applied to all data presented here (i.e. routine reports and long-time series data). Firstly, any measurements flagged as *bad* within the NetCDF files (based on those variables containing *qual* in the name in European Space Agency (2019)) or that are from an orbit identified as biassed are removed. In addition, the thresholds on the measurements/corrections in Table 1 are used to remove outliers. As an example of some of the information contained in the monthly reports, Table 1 also provides the percentage of data removed for the QC criteria for GOP in November 2023. Finally, for 1 Hz data to be considered usable, the number of 20 Hz datapoints in the stack must be 10 or above.

Monthly reports are provided with a latency of 1–2 months to allow for the collection of GOP and validation data. As such a small number of monthly reports are available for Baseline D but consideration needs to be made of the latency of the different products to account for when the new Baseline reports are appropriate. An ongoing reprocessing of Baseline D will enable a fuller study of Baseline D when sufficient data are available.

For each routine report, based on the predicted ground tracks, the theoretical number of 1 Hz data points are calculated. This theoretical upper value alongside the number of data points that pass QC (referred to as science-valid) allow us to calculate the percentage of valid data. Fig. 2, which is taken, as an example, from the November 2023 monthly report, shows the percentage of valid SSHA data

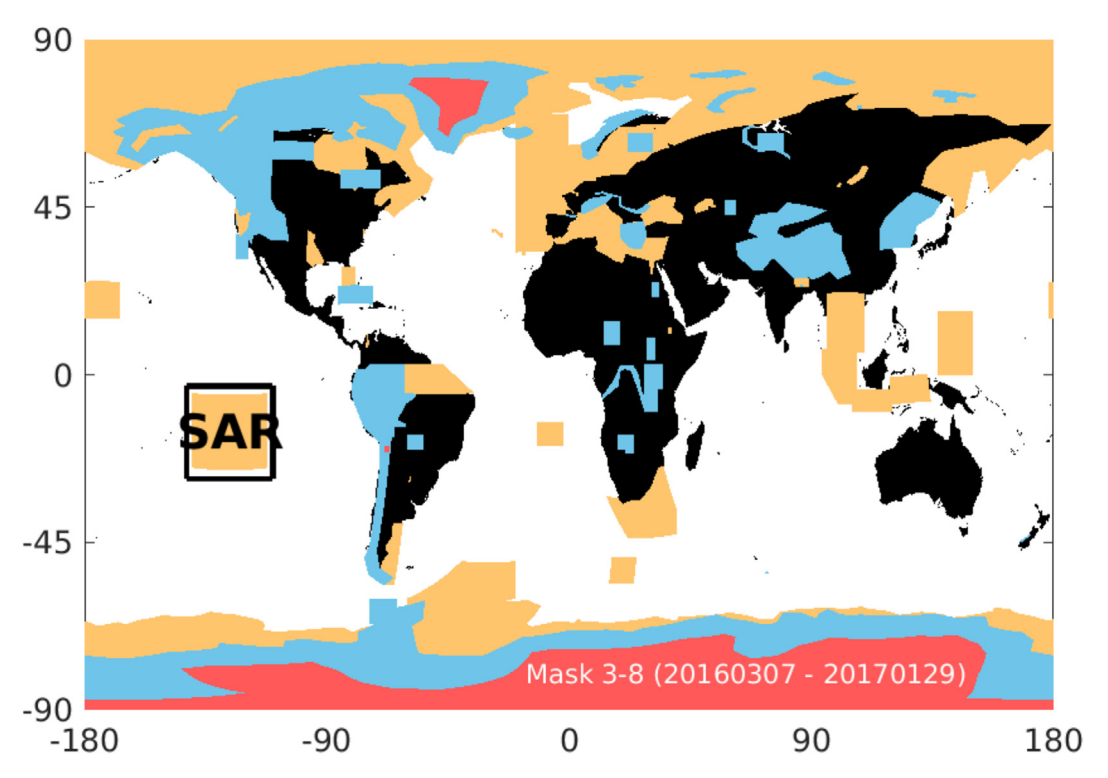


Fig. 1. Example of CryoSat-2 mode mask (version 3–8; https://earth.esa.int/eogateway/instruments/siral/geographical-mode-mask). White is Low Resolution Mode (LRM) over ocean; red is LRM over land/ice sheets; orange is Synthetic Aperture Radar (SAR); and blue is SARIn (SAR – interferometric mode). The black box labelled SAR is discussed in Section 3.3.

Table 1
Routine quality control of SIRAL data for routine reporting, any values outside of these ranges are excluded from the analyses. The last column provides the percentage of data excluded in November 2023.

Parameter	Minimum threshold	Maximum threshold	Sample Percentage (November 2023)
SSH anomaly	-3 m	3 m	0.2
Standard deviation of SSH anomaly	0 m	0.20 m	1.0
Inverse barometer correction	−2 m	2 m	0.0
Wet tropospheric correction	−0.5 m	−0.001 m	0.0
Dry tropospheric correction	−2.5 m	−1.9 m	0.0
Ionospheric correction	−0.4 m	0.04 m	0.0
Sea state bias	−0.5 m	0 m	0.1
Sigma0	7 dB	30 dB	0.2
Standard deviation of sigma0	0 dB	0.23 dB	4.1
SWH	0 m	15 m	0.0
Standard deviation of SWH (1-Hz block)	0 m	1 m	1.3
Altimeter wind speed	0 m/s	30 m/s	0.0

for every day in the month for NOP, IOP and GOP. For all three products the percentage is on average over 70 % with a slightly higher standard deviation for NOP (10.1 %) compared with IOP and GOP (both 7.3 %). This is perhaps not surprising given the timeframe for delivery as discussed in the next section. It should be noted that the percentage of science-valid for IOP and GOP are not always identical (e.g. for March 2024 the values are 72.2 % and 71.6 % for IOP and GOP respectively).

## 2.1. Latency

The latency requirements for COP products relate to the different user requirements and meeting these requirements is monitored through the routine reports. As an example, Fig. 3 shows, for November 2023, the latency for NOP, IOP and GOP against their target delivery windows of 3 h, 3 days, and 30 days respectively. IOP and GOP are clearly providing the data within the target windows whilst

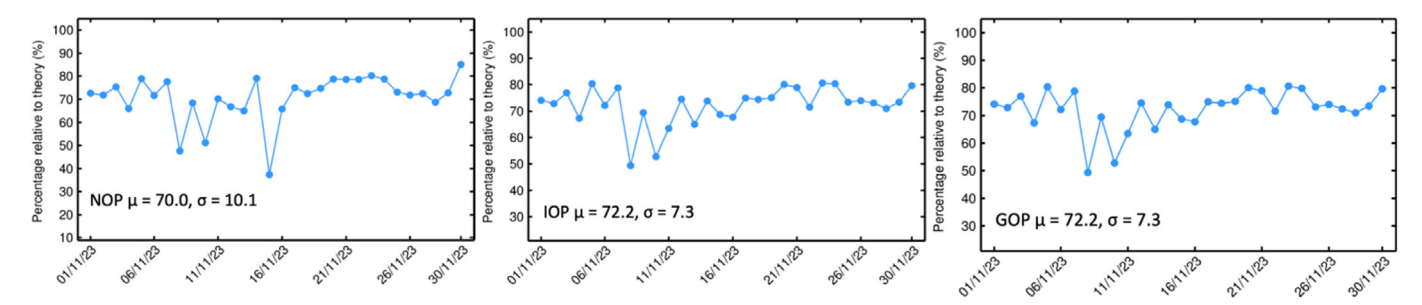


Fig. 2. Percentage of science-valid 1 Hz SSHA records over ocean and lakes relative to theory for each day in November 2023 for (left to right) NOP, IOP and GOP. The means ( $\mu$ ) and standard deviations ( $\sigma$ ) of the percentages are also shown.

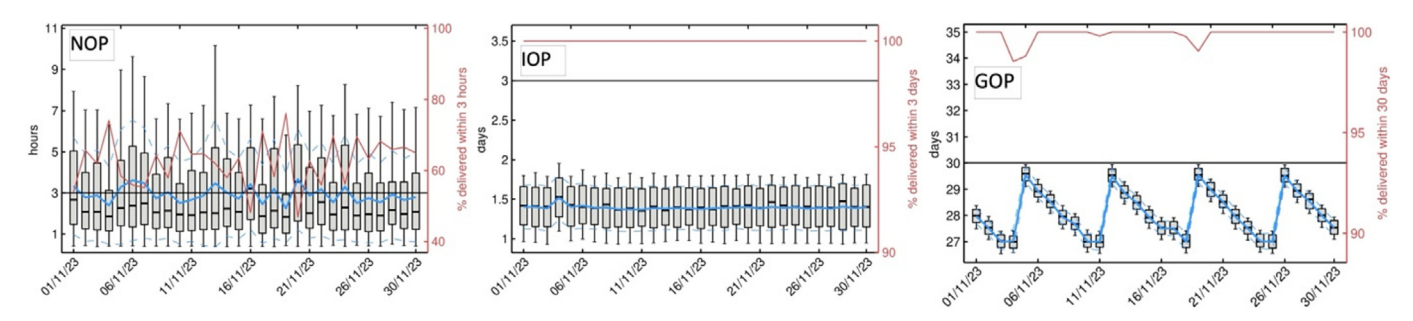


Fig. 3. Box-and-whiskers plot for the (left to right) NOP, IOP and GOP latency showing for each day in November 2023 the first and third quartiles (bottom and top of the grey box), the median (thick black in box), the 5 % and 95 % percentiles (lower and upper whiskers), the mean (solid, blue line) and the mean ± 1 standard deviation (dashed, blue line). The percentage of records delivered within 3 h (NOP), 3 days (IOP) and 30 days (GOP) is also shown (red, right y-axis). The horizontal black line denotes the latency target.

~60–70 % of NOP is delivered within the 3-hour target. The clear periodicity for GOP is expected behaviour due to the data generation model, in particular, dependency on availability of orbit files. These values are typical of other months and the information is available in the reports.

## 3. Data and methods

The data used here are based on along-track, 1 Hz GOP (Level 2) and if not explicitly stated are only LRM. The data period covered is from 1 January 2011 to 31 December 2023. All data have the QC procedures discussed above applied. There are a number of times for which there are no data available, these can be found detailed at https://earth.esa.int/eogateway/missions/cryosat/data/data-unavailability-periods.

As many validation data sources are based on gridded values, the along-track C2 data were averaged over gridded datasets. A number of resolutions of monthly, gridded QC GOP data were tested (0.5°, 1.0°, 2.5°, 5° and 10°). Mostly 2.5° resolution provided the necessary balance of representativeness and sufficient data, but this will be specified in the text. In a similar way, both mean and median values were calculated but here we present only means as there was little difference. In addition, the gridded means were calculated separately for measurements from ascending and descending passes. Details of the validation data sources used for comparison are given in Sections 3.5–3.8.

## 3.1. SSHA calculation

It should be noted that the combination of corrections used below (and in the routine reports) are not identical to the calculation of SSHA in the GOP data files supplied by ESA (ssha 01 ku). Further details of the data product calculations and corrections can be found in the product handbook supplied by ESA (2019). The differences with ssha 01 ku are the use of CNES-CLS15 for MSS and FES2014b for the tide correction. Here the corrected range (CR) is calculated as the range corrected for: wet (WTC; Fernandes and Lazaro, 2016) and dry tropospheric (DTC; from ECMWF) delays; ionospheric path delay (JPL Global Ionosphere Maps – GIM); and sea state bias (SSB) simplified below in Eq. (1). SSB is computed using CryoSat data according to the methodology in Tran (2015) data from the same mode are used for LRM (/PLRM), and SAR, while the SSB from LRM is used for SARIn.

$$CR = range + WTC + DTC + GIM + SSB$$
 (1)

Sea surface height (SSH) is found by correcting CR for tides (solid Earth, ocean, loading and pole) and atmospheric pressure (DAC; dynamic atmospheric correction) and subtracting from altitude of SIRAL (Alt) as per Eq. (2). DAC can also remove wind effects but not in this case as the comparison is for monthly data and, for periods longer than 20 days, the DAC defaults to an inverse

barometer correction. The total geocentric ocean tide is solution 1 provided in the GOP NetCDF files (GSFC; GOT).

$$SSH = Alt - CR - GOT - solid Earth tide$$

$$- geocentric polar tide - DAC$$
 (2)

SSHA is then simply found by subtracting MSS (DTU15; Andersen, 2010, Andersen, 2022, Andersen and Knudsen, 2009) from SSH. The values of SWH and WSP are taken directly from the variables in the GOP NetCDF files.

## 3.2. Trend analyses

The method described below was used to calculate trends in SSHA, SWH and WSP for GOP alongside some of the additional data both globally and regionally (e.g. using gridded C2 data). Let  $X_t$  denote the value of the variable X at time step t, where X can refer to SSHA, SWH, or WSP. The regression model that we use to calculate the trend and amplitudes of the annual and semi-annual cycles can then be written as:

$$X_t = D + Ct + \sum_{i=1}^{2} [B_i \cos(\omega_i t) + A_i \sin(\omega_i t) + e_t]$$
 (3)

where D is an intercept, C is the trend,  $A_i$  and  $B_i$  for i=1,2, are constants,  $\omega_i$  is angular frequency ( $\omega_1$  for the annual cycle and  $\omega_2$  for the semi-annual cycle), and  $e_t$  is an error term. In ordinary least squares (OLS), the errors  $e_t$  are assumed to be serially uncorrelated (among other assumptions). For climatic variables, however, this assumption is often violated, which causes OLS to produce overly optimistic uncertainty estimates. To account for serial correlation in the residuals, we model  $e_t$  as a first-order autoregressive process (AR1):

$$e_t = \rho e_{t-1} + u_t \tag{4}$$

where  $\rho$  is an autoregressive coefficient that controls the degree of temporal autocorrelation, and  $u_t$  is white Gaussian noise. To fit the regression model we adopt a Bayesian approach, and thus assign prior distributions to all the unknown parameters of the model. Estimates are obtained by numerically sampling from the so-called posterior distribution using a Gibbs sampler. The general structure of the model as well as the sampling approach are the same as described by Chib (1993) and we defer to this study for full details.

Once estimates of the regression coefficients are available, the amplitudes of the annual and semi-annual cycles  $(\alpha_i, \text{ for } i=1,2)$  are calculated as:

$$a_i = \sqrt{A_i^2 + B_i^2} \tag{5}$$

Because estimates of  $A_i$  and  $B_i$  are in the form of samples from their joint posterior distribution, propagating their uncertainties through Eq. (5) is automatic (i.e., the

samples that results from applying Eq. (5) to each sample of  $A_i$  and  $B_i$  account for any dependencies in  $A_i$  and  $B_i$ ). It is worth noting that the estimates of the regression coefficients from this regression model are very similar to those derived from OLS. However, in the presence of strong serial correlation, the model with autocorrelated errors yields more realistic uncertainty estimates.

For the global datasets, the results presented here include weighting the means by the cosine of the latitude in order to take into account the density of ground points. Such an approach does not impact significantly on the trend analyses (not shown).

#### 3.3. LRM-SAR transition

In order to look at issues related to the SAR-LRM transition (bias), successive differences in SSHA, SWH and WSP with a maximum temporal separation of 2 s were calculated. These values can then be averaged over each month split by the difference in the operating mode flag. This aspect of the work focusses on the SAR box shown in Fig. 1 bounded by [28°S 3°S] and [142 W 110 W]. For each variable and month, there are then means corresponding to three classes: from LRM to SAR; from SAR to LRM; and no change in mode.

## 3.4. Ascending-descending bias

To reduce noise in the results, this part of the study used a grid resolution of  $10^{\circ} \times 10^{\circ}$ . For each grid cell the difference in mean monthly ascending minus mean monthly descending passes was calculated for SSHA, SWH and WSP. The results were further averaged across all longitudes and months to provide binned averages in  $(10^{\circ})$  latitude bins.

#### 3.5. Global mean sea level data

The current ocean reference altimetry mission is Sentinel-6 Michael Freilich and like its predecessors, which have been in orbit for over 30 years, has a repeat orbit of ~10 days (e.g. Donlon et al., 2021). This provides a different sampling of the oceans compared with the unique orbit of C2 and hence an alternative view of GMSL. Here we use two readily available estimates of GMSL referred to as Colorado (Sea Level Research Group and University of Colorado, 2023) and Beckley (Beckley et al., 2017; Beckley et al., 2021).

## 3.6. PSMSL data

Comparisons of GOP and selected tide gauge locations is routinely presented in the monthly reports. Here, a more comprehensive comparison was undertaken using data from the Permanent Service for Mean Sea Level (Holgate et al., 2013; Permanent Service for Mean Sea Level (PSMSL), 2023). Specifically, we have used those tide

gauges that have been reduced to the Revised Local Reference (RLR). For tide gauge data for the same time period (2011–2023) as C2, additional criteria were applied to ensure sufficient data were of a suitable quality at each location. These criteria included ensuring that there were data for each of the 156 months that passed the PSMSL quality flags and that no station had more than 12 occasions with more than a week of missing data throughout the period.

This resulted in 116 tide gauges. For consistency with the altimetry data, atmospheric pressure effects on sea level were removed from the tide gauge records using data from the NCEP/NCAR reanalysis (Kalnay et al., 1996) and assuming an inverse barometer effect. The linear trend term from each tide gauge of these was then removed. If a grid cell contained more than one tide gauge, then the longest period of overlapping data from the two gauges were revised to have the same mean. This was repeated until all the gauges in a grid cell had the same origin and the values for each month were then averaged across tide gauges. Before calculation of the (Pearson) correlations, the linear trends in both the C2 and averaged PSMSL data have been removed.

## 3.7. WaveWatch III data

The routine monthly reports incorporate a comparison of SWH from GOP with the Pacific Islands Ocean Observing System version of the WaveWatch III model (WW3; https://www.pacioos.hawaii.edu/waves/model-global/#about). This is a global 5-day, hourly forecast of SWH at ~50 km resolution that is run daily (Cheung, 2010 (updated 2021)). For each month in the study period, the SWH for each model location is taken as the mean, which in turn is interpolated onto the same 2.5° grid as GOP data. The interpolation is using the cubic option within the MATLAB *interp2* function (The MathWorks Inc., 2020).

## 3.8. ERA5 data

ECMWF 5th generation reanalysis (ERA5) monthly averaged wind speeds (Hersbach et al., 1940) were obtained from https://cds.climate.copernicus.eu/ on 7th March 2024. ERA5 wind speeds have a horizontal resolution of 0.25° and we have calculated the 10 m wind speed from the supplied eastward and northward components. The data are interpolated to the 2.5° grid using the same method as for WW3.

## 4. Results

## 4.1. Trend analyses

#### 4.1.1. Global trends

Fig. 4 shows the time series for monthly, global mean SSHA, SWH and WSP from the QC GOP LRM data. This is shown for all data and split by satellite direction (i.e.

ascending or descending passes). In the SSHA/GMSL plot the timeseries are also shown for the Colorado and Beckley datasets. The two external GMSL timeseries have had their means shifted to match the mean of the C2 SSHA. The legends in Fig. 4 provide the OLS and Bayesian trends and uncertainties from the latter approach: the best combination is that of OLS trend and Bayesian uncertainty (i.e. standard errors) and these are the values reported here. For GMSL, the trend from C2 is  $4.2 \pm 0.3$  mm/year which is marginally lower than that from Colorado or Beckley (4.  $5 \pm 0.1$  mm/year and  $4.3 \pm 0.1$  mm/year respectively) with a larger uncertainty.

All three estimates of trend agree within the calculated uncertainties. Although GMSL from descending passes is generally higher than that from ascending passes the trends are similar. The trend for GMSL from ascending passes is  $4.3 \pm 0.3$  mm/year compared to  $4.2 \pm 0.2$  mm/year for descending and as such agree with the combined GOP timeseries and the other timeseries. Further results referring to the ascending versus descending issue are presented in Section 4.3.

There are no significant trends in GOP LRM SWH (Fig. 4b) for either all data or split by satellite direction (all trends are  $0.0 \pm 0.0$  m/year). There is also no obvious bias between ascending and descending passes; any differences are probably simply due to sampling.

Finally, Fig. 4c shows the trends in GOP LRM WSP with an overall trend of  $3.3 \pm 0.2$  (cm/s)/year. As with GMSL, there is a tendency for higher values from descending passes along with a higher trend of  $3.6 \pm 0.3$  (cm/s)/year. The trend from ascending passes is lower at  $3.1 \pm 0.3$  (cm/s)/year although like all the trends is not significantly different from the others.

## 4.1.2. Regional trends

Using the same methodology as for global trend analysis, Fig. 5 shows the patterns in trends in C2 SSHA, SWH and WSP based on OLS. Only trends that are more than the uncertainty from zero are shown using the uncertainties based on the Bayesian methodology. It should be noted that Fig. 5 shows LRM only and so the Pacific SAR box (shown approximately by the box labelled SAR in Fig. 1) and North West European Shelf show zero trends (i.e. white). The Pacific SAR box had changed size with different acquisition masks and as only locations with full timeseries are considered Fig. 5 represents the combined maximum extent of all incarnations. Fig. 5 also shows the results from ERA5 WSP based on the same methodology but at the higher, native spatial resolution.

For SSHA, in general, the trends are positive with a few notable exceptions particularly in Indian Ocean and Northwest Pacific. This is in general agreement with the shorter timescales seen in Fig. 5 in Banks et al. (2023) from CryoSat (2011–2020) and the European Space Agency Climate Change Initiative Sea Level version 2 (Legeais et al., 2018).

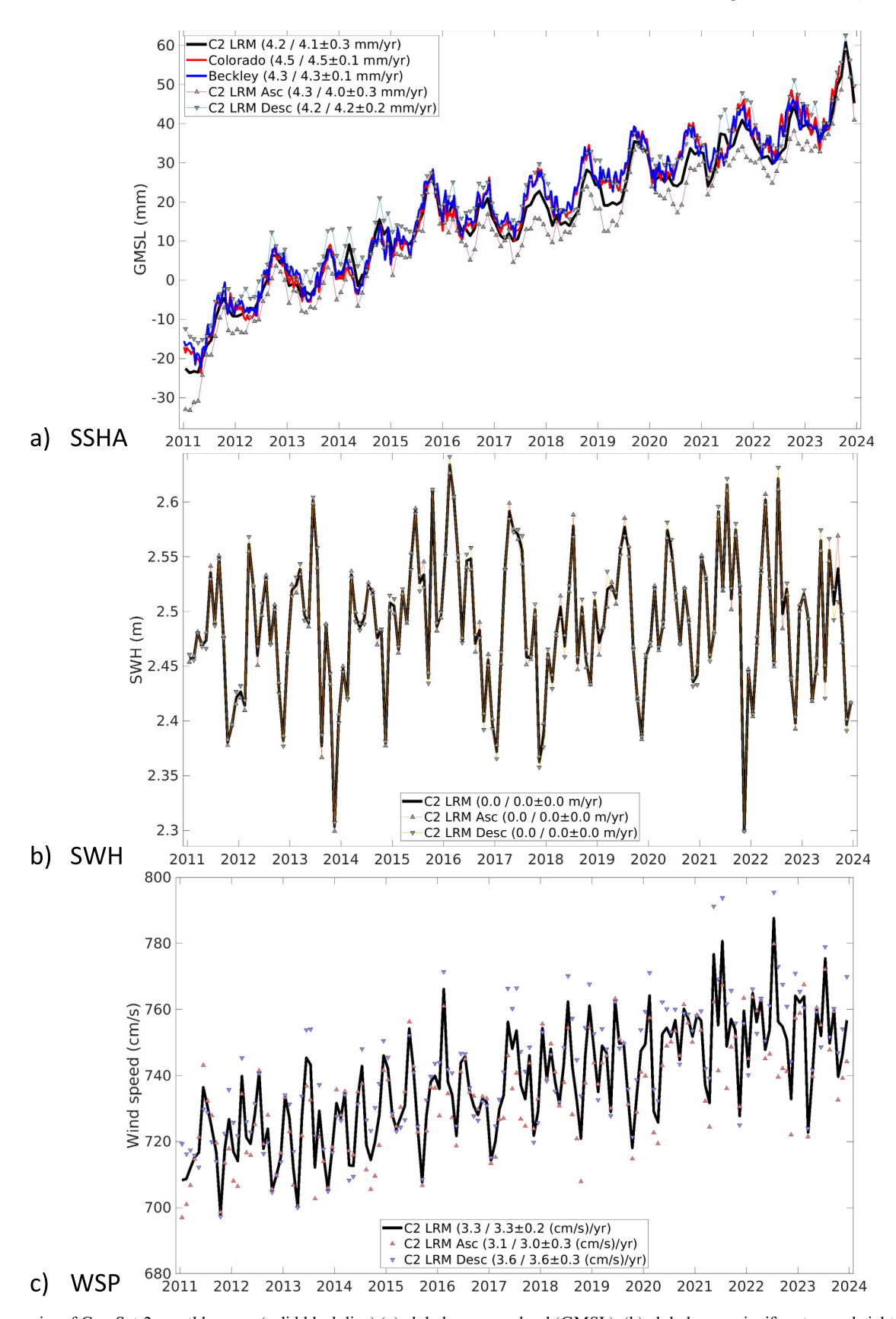


Fig. 4. Time series of CryoSat-2 monthly mean (solid black line) (a) global mean sea level (GMSL); (b) global mean significant wave height (SWH); and (c) global mean wind speed (WSP). Downward pointing triangles show the same just for descending passes and upward pointing triangles show for ascending passes. Legend includes ordinary least squares trend/Bayesian Trend and uncertainty. (a) also includes GMSL trends from Colorado (solid red line) and Beckley (solid blue line) as defined in the main text.

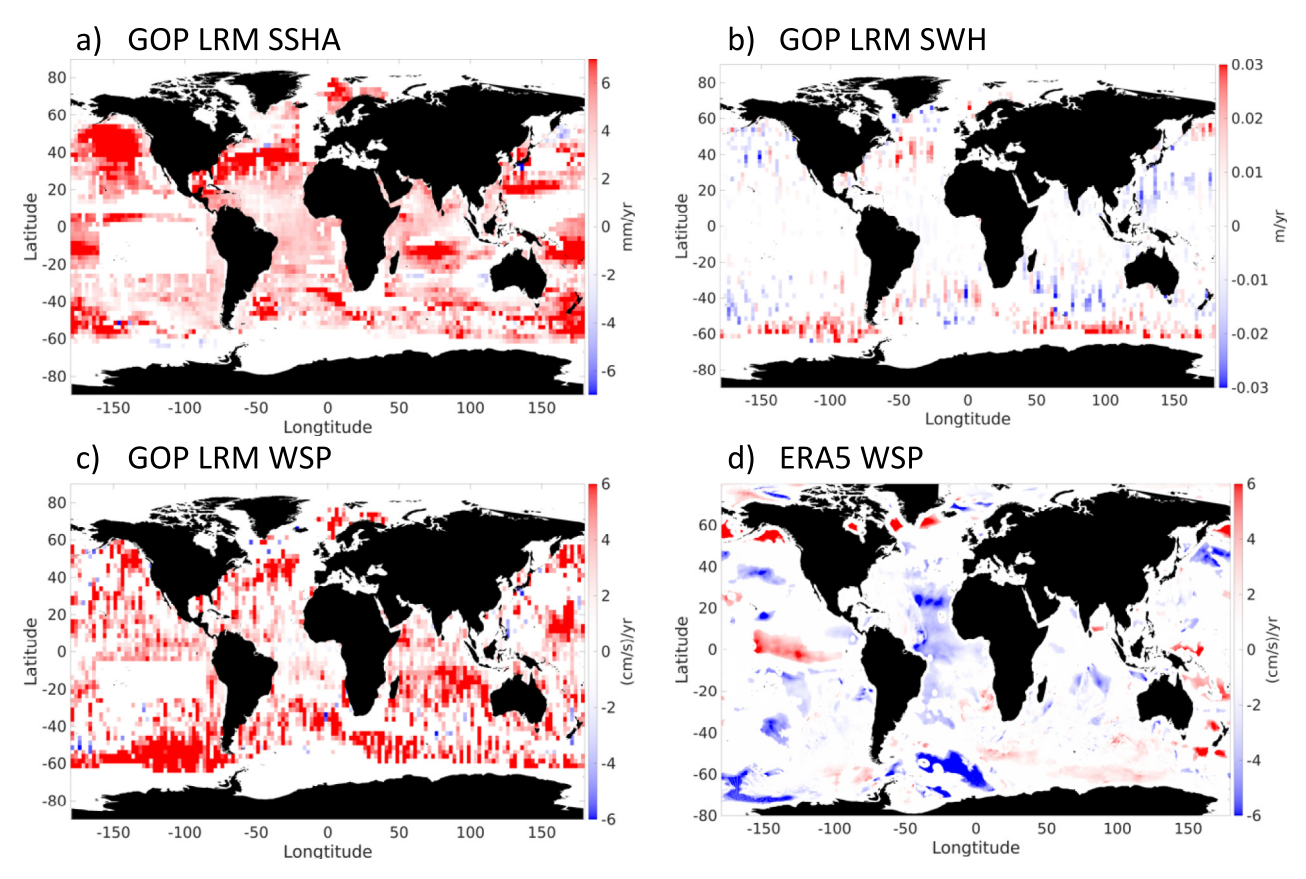


Fig. 5. Trends in CryoSat GOP LRM (a) sea surface height anomaly (SSHA); (b) significant wave height (SWH); (c) wind speed for the period 2011–2023 on  $2.5^{\circ} \times 2.5^{\circ}$  grid; (d) trends for ERA5 wind speed  $(0.25^{\circ} \times 0.25^{\circ}$  grid resolution).

For SWH, except for the Indian Ocean, the geographical pattern in trends is similar to the results from Fig. 2A in Young and Ribal (2019) for the period 1985–2018 based on a global assessment of satellite data. The mostly positive trends for WSP in C2 do match the results from (Fig. 1A in Young and Ribal, 2019) for the period 1985–2018 but the negative trends seen in the other study (centred around Southeast Asia) are not clear in the C2 data. The patterns in C2 SWH, and to a lesser extent WSP, show some evidence of tracks (*trackiness*): this suggests that the trends may be overly influenced by individual events (e.g. storms).

The patterns in WSP from C2 do not correspond to those from ERA5; the latter showing distinct regions of WSP decreasing not seen in C2. It should be noted that C2, like other satellite altimeters, is unable to measure low values of WSP (<~2 m/s) and likely impacts on the calculated trends. Note that ERA5 are monthly means so it is not possible to simply philtre out low WSP in order to match the C2 WSP.

#### 4.2. LRM-SAR bias

For each variable, Fig. 6 shows the timeseries of the monthly, mean successive differences for: no change in mode; change from SAR mode to LRM; and change from LRM to SAR mode for the study region labelled as SAR in

Fig. 1. The versions of the mode mask are labelled and for versions where there is no SAR box in the region (i.e. 3.2, 3.7 and 4.0) there are no data points. The number of measurements for any given month are low (between 10 and 80) and this is reflected in the 95 % confidence intervals shown in Fig. 6. The 95 % confidence intervals for the *no change* category are essentially zero so are not shown. If the time window allowed for successive differences was relaxed to 5 s rather than 2 s (not shown), then the maximum number per month is still less than 80 but obviously the spatial separation of points is much higher.

As discussed above, the size of the SAR box varies amongst versions of the mode mask. However, the variation in the differences in Fig. 6 using any given version of the SAR box can be greater than the variation amongst mode masks with different sized SAR boxes.

#### 4.3. Ascending versus descending passes

As seen above (e.g. Fig. 4), there are biases in measurements from ascending versus descending passes and these are explored in further detail here. In addition to considering the temporal evolution of the ascending minus descending signal globally (within 66°S–66°N), the timeseries are presented by hemisphere (Fig. 7). For all three variables, strong variable signals are visible in all three timeseries.

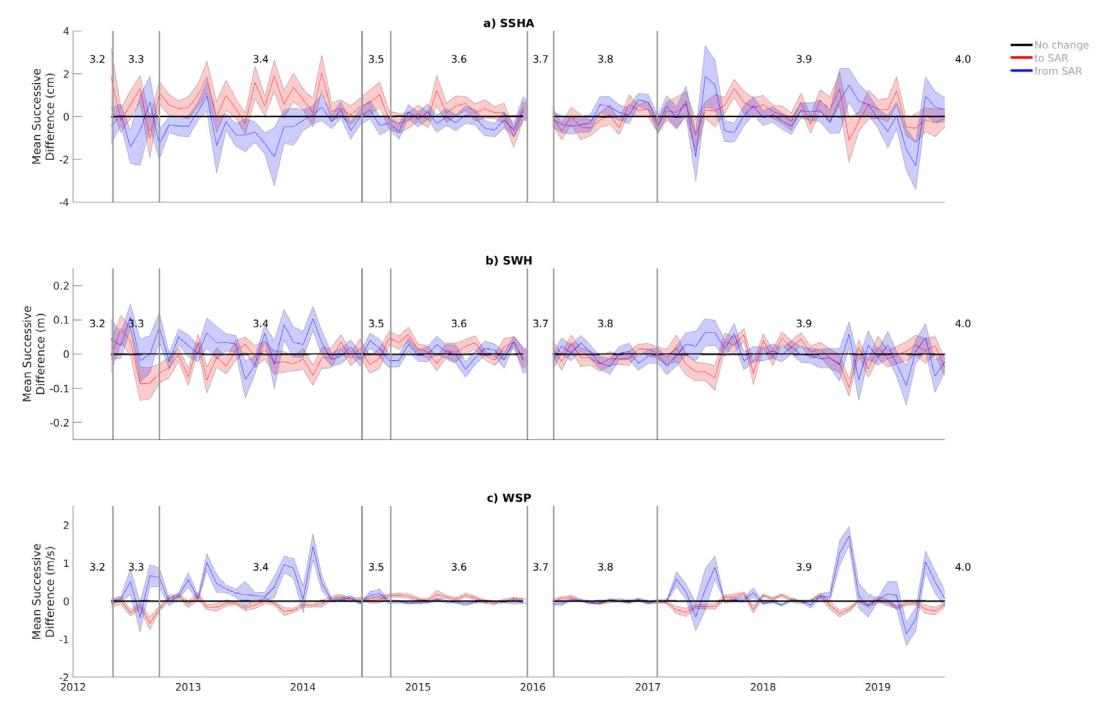


Fig. 6. Time series of monthly mean of successive (along track) differences for (a) SSHA, (b) SWH and (c) WSP. No change in mode is shown by solid, black lines, solid, blue line is change from SAR to LRM and solid, red line is change from LRM to SAR. The shading shows the standard error of measurement for changes of mode. The divisions in the timeseries relate to changes in mode mask (versions 3.2–4.0).

For SSHA, the bias in monthly mean ascending minus monthly mean descending tends to be positive in the Northern Hemisphere (i.e. ascending greater than descending on average) whereas it is always negative in the Southern Hemisphere. The magnitude of the seasonal cycle in SWH bias in Fig. 7 overlaps the zero line and as such supports the findings in Fig. 4 that suggest there is no significant bias. The results for the bias in WSP in Fig. 7 are a combination of the other two variables with strong seasonal cycles but notable biases especially for Southern Hemisphere. It should be noted that Fig. 7 is for LRM data only.

## 4.4. PSMSL

The correlations of monthly PSMSL tide gauge data with 1° (average) gridded C2 SSHA are shown in Fig. 8a for LRM and SAR data (where available given the mode mask). Results from other resolutions (0.5°, 2.5°, 5° and 10°) of the mean gridded C2 SSHA were calculated but there was a peak in the number of observations for the one-degree resolution. All the significant correlations were positive (between 0.24 and 0.94 for LRM and 0.26 and 0.84 for SAR) with a mean of 0.67 for LRM and 0.59 for SAR. For LRM, the mean correlation is 0.66 for 0.5° resolution, 0.67 for 2.5°, 0.65 for 5° but drops to 0.60 for 10°.

The inset in Fig. 8a shows the relationship of LRM versus SAR correlation coefficients, where both are available split by whether or not they are significant. Particular care must be taken when considering these as the number of

samples are limited. The distributions of the significant corelations are provided in Fig. 8b for the one-degree C2 grid. It is hard to determine any differences in the distributions as there are too few SAR locations to be meaningful.

#### 4.5. Significant wave height

In order to investigate C2 SWH, results from a comparison with the WW3 model output described above are reported here. As with other variables in this study it should be remembered that this is using monthly gridded averages (in this case 2.5° resolution). Fig. 9a shows the bias (mean) between C2 SWH and WW3 SWH globally and split by hemisphere. In general, with a notable exception between mid-2012 and early 2015, C2 SWH is ~0.1–0.2 m lower than SWH from WW3. It is not possible to identify whether this anomalous period is due to issues with one or more of the following: C2 data, WW3 model output or geophysical causes. This period does correspond to specific versions of the mode mask (3.3–3.5) and a period of lower numbers of LRM measurements (~10 % fewer; not shown) which was considered as one possible cause.

In contrast, Fig. 9b shows a consistent pattern in the correlation between monthly, mean SWH from C2 and from WW3. Globally and for the Southern Hemisphere there is a correlation of  $\sim 0.85$  with a seasonal maximum variability of  $\sim 0.05$ . For the Northern Hemisphere the seasonal cycle includes sharp troughs, usually two per year, where, for some years, the correlation decreases to below 0.7.

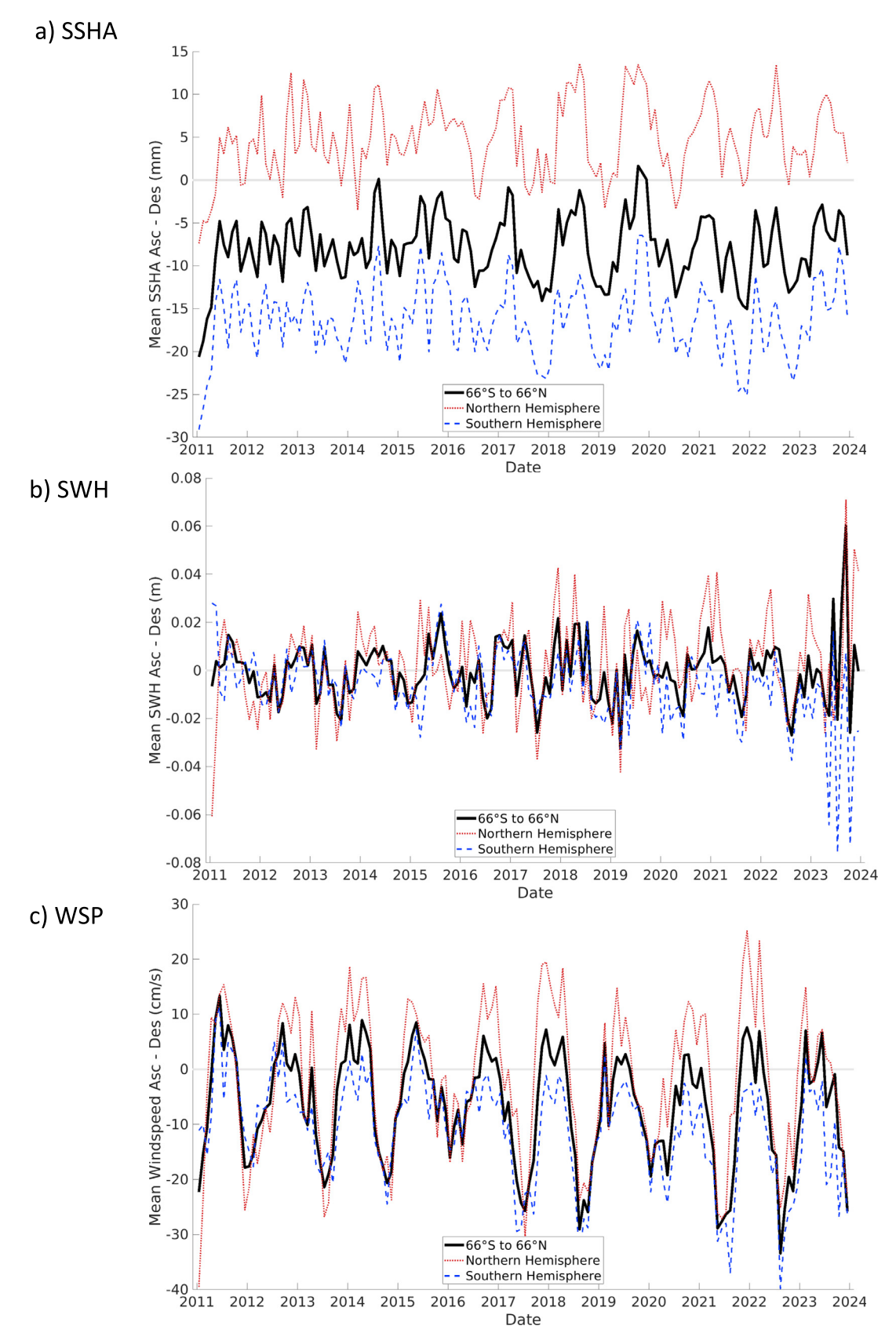


Fig. 7. Monthly mean ascending minus monthly mean descending for: (a) sea surface height anomaly (SSHA); (b) significant wave height (SWH); and (c) wind speed (WSP). Solid, black lines are global (66°S–66°N), dotted, red lines are Northern Hemisphere and dashed, blue lines are Southern Hemisphere. Data are LRM only.

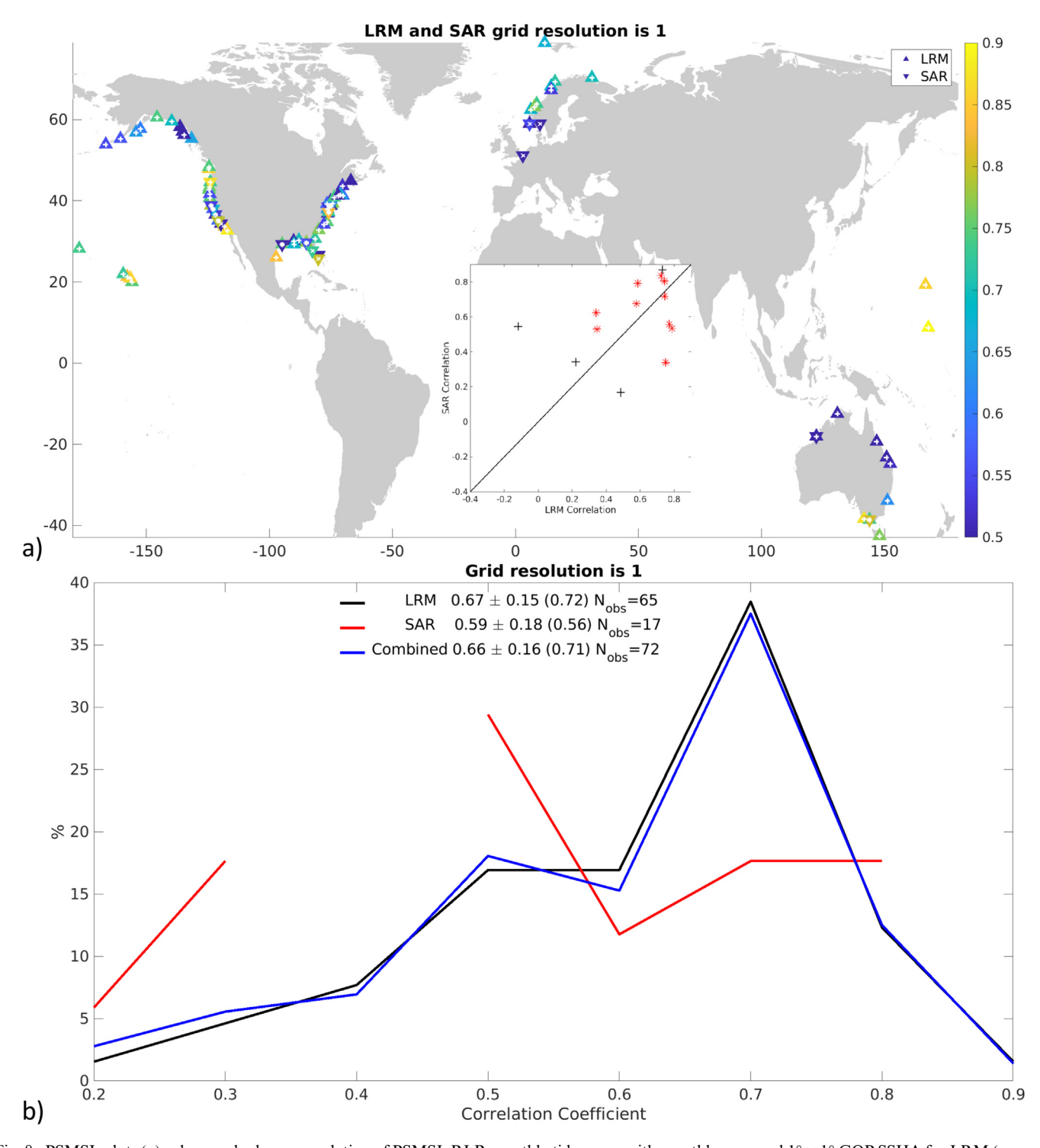


Fig. 8. PSMSL plots (a) colour scale shows correlation of PSMSL RLR monthly tide gauge with monthly averaged  $1^{\circ} \times 1^{\circ}$  GOP SSHA for LRM (upward pointing triangle) and SAR (downward pointing triangle). Note: It is possible for a location to have both upward- and downward-pointing triangles. Significant correlations (95 %) are indicated by white plus (+) for LRM and white x for SAR. Inset shows correlation of tide gauge with LRM (x-axis) and SAR (y-axis), where red asterisks indicate both correlations are significant (95 %). (b) Distribution of significant correlation coefficients using same as (a). Black line shows LRM, Red line is SAR, and blue line is all data. Legend provides mean  $\pm$  standard deviation and number of observations (N<sub>obs</sub>) for each mode(s).

To look at the relationship between monthly, mean C2 SWH and WW3 SWH further, Fig. 10 shows C2 SWH as a function of C2 SWH minus WW3 SWH globally and split by hemisphere. There are no clear differences in

the pattern amongst the subplots. The vast majority of data sits close to the zero bias line suggesting good agreement between C2 and SWH. Considering the pattern at lower intensity suggests that at low (C2) SWH there is more likely

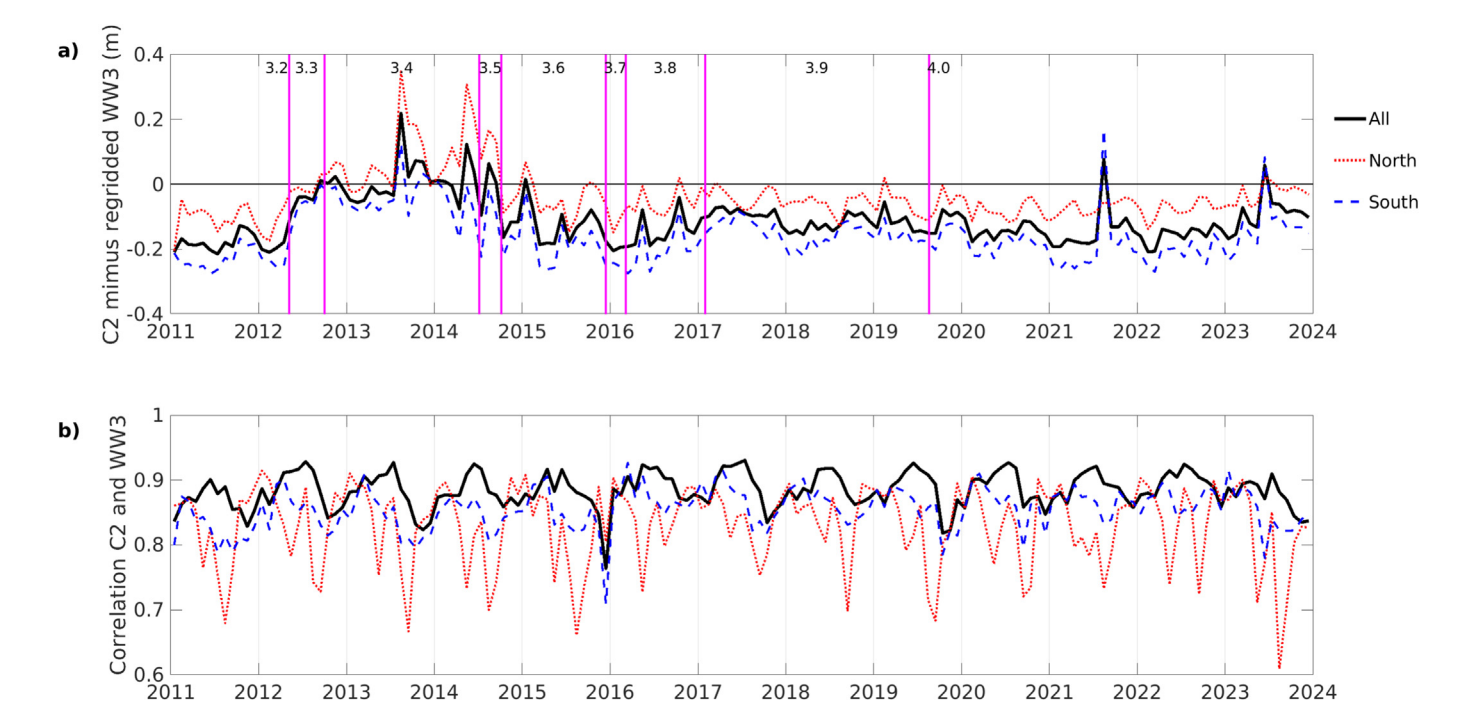


Fig. 9. Timeseries of (a) Monthly mean CryoSat (C2) significant wave height (SWH) minus monthly mean WaveWatch3 (WW3) SWH; and (b) correlation between monthly mean C2 SWH and WW3 SWH. For both plots, solid, black lines are for global study region (65°S–65°N); dotted, red lines are Northern Hemisphere; and blue, dashed lines are Southern Hemisphere. The magenta lines in a) correspond to the labelled mode mask version.

Date

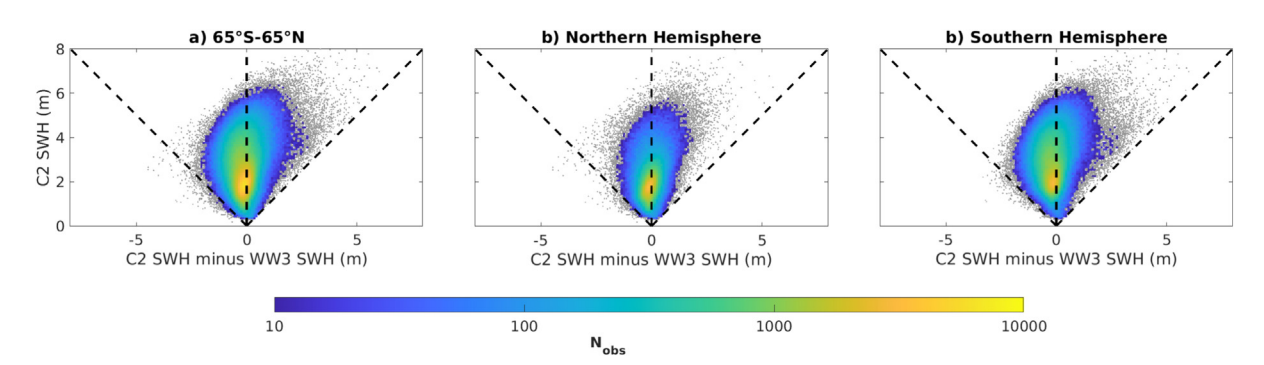


Fig. 10. 2-D histograms of 2.5° gridded, monthly, mean CryoSat significant wave height (SWH) minus monthly mean WaveWatch3 (WW3) SWH (x-axis) against monthly, mean CryoSat SWH (y-axis) for (a) global study region (65°S–65°N); (b) Northern Hemisphere; and (c) Southern Hemisphere. Histogram bins are 0.1 m in both dimensions and measurements in bins with less than 10 measurements are shown as grey dots.

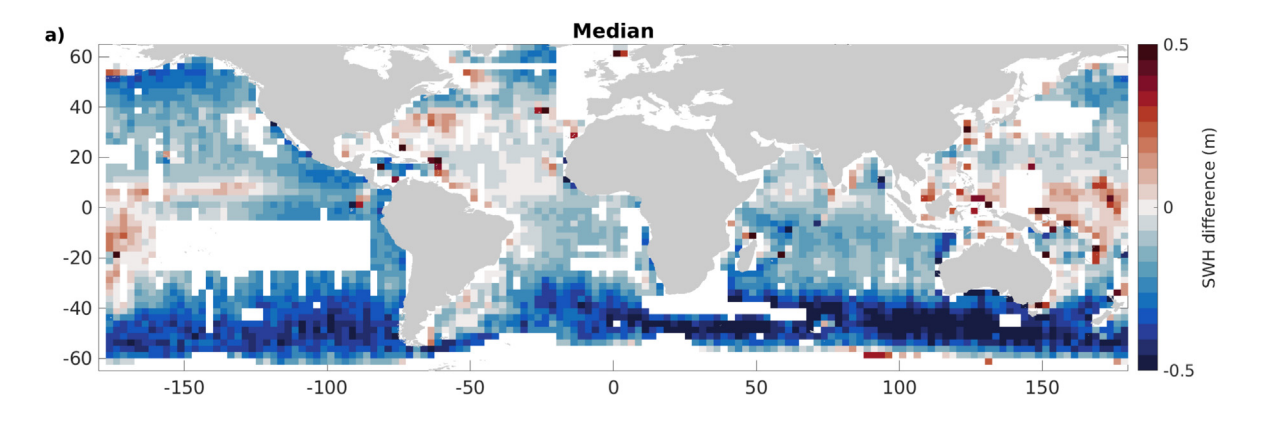
to be a negative bias (WW3 tends to be higher than C2), whereas at higher SWH the opposite is the case with a tendency for C2 SWH to be higher than WW3. It should be noted that the colour scale in Fig. 10 is logarithmic and this pattern is clearer in the outliers than the bulk of the data. In the Northern Hemisphere there is a slight slope to the bulk of the data (i.e. yellow area), but this may be as a result of the lower number of data pairs compared to the other two subplots.

Looking at the spatial variation of the differences averaged (median) over the full timeseries (Fig. 11) shows that the situation is more complex. Fig. 11a suggests that at low latitudes (generally lower sea state) the bias is low as is (from Fig. 11b) the variability of the bias. In the Southern

Hemisphere between about 35°S and 60°S, the bias is higher in magnitude with WW3 higher than C2 SWH with more variability in the bias. Whereas at lower latitudes and in the Northern Hemisphere, Fig. 11 suggests that WW3 and C2 are similar in magnitude or that the sign of the bias is reversed (i.e. C2 SWH > WW3 SWH).

## 4.6. Wind speed

In a similar manner to the previous section, Fig. 12 provides 2-d histograms of the WSP bias between ERA5 and C2 globally and by hemisphere. There is a clear relationship that at higher wind speeds there is a negative bias (i.e. ERA5 WSP is higher than C2 WSP). At lower WSP,



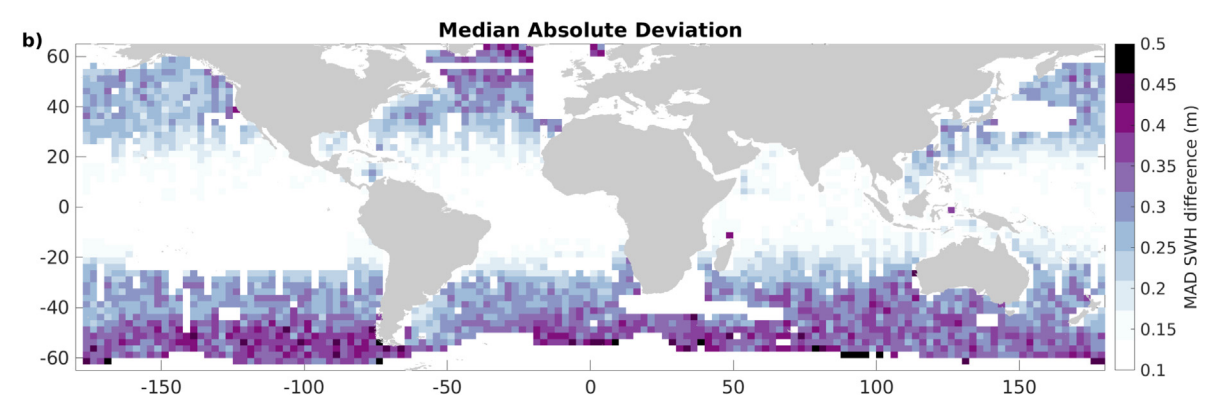


Fig. 11. Geographical plot of the (a) median and (b) median absolute deviation (MAD) of monthly CryoSat-2 (C2) significant wave height (SWH) minus WaveWatch3 (WW3) SWH for 2011–2023.

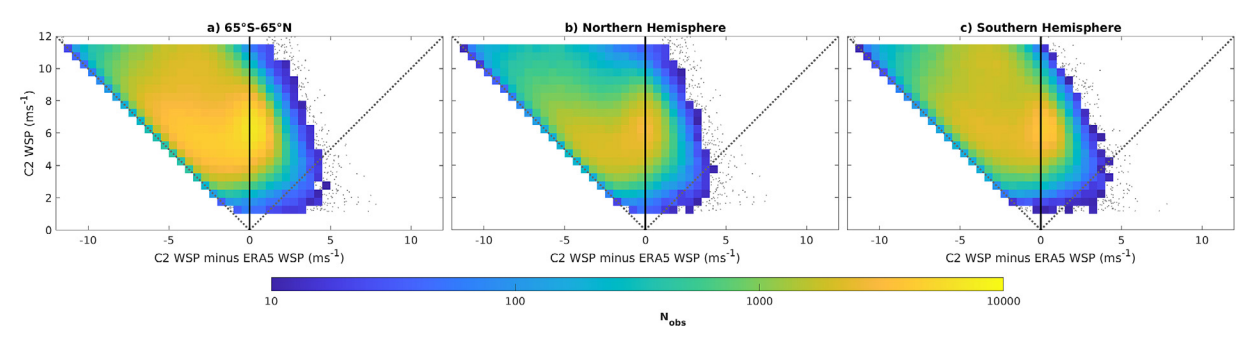


Fig. 12. 2-D histograms of CryoSat-2 wind speed (WSP) as a function of CryoSat-2 WSP minus ERA5 WSP. Histogram bins are 0.5 ms<sup>-1</sup> in both dimensions and measurements in bins with less than 10 measurements are shown as grey dots.

the opposite is the case (i.e. C2 WSP is higher than ERA5 WSP) although this is not as pronounced. It should be noted that altimetry is not able to recover low WSP (<~2 m/s) from the waveforms and this is the reason for the lack of low WSP data in Fig. 12. It is worth noting that the results for WSP from ascending and descending passes provide similar patterns (not shown).

#### 5. Discussion

In this study we investigated the quality of C2 SSHA, SWH and WSP over a thirteen-year period (2011–2023

inclusive). This work complements the findings available in the series of routine reports discussed in Section 2. These routine reports (daily for NOP/IOP and monthly for all products) can be used to identify any issues or changes in the availability and quality of the COP.

A number of the additional results reported above were based on mean, monthly gridded values of SSHA, SWH and WSP in order to compare with validation/comparative data sources. Unlike other altimeters with repeat orbits of 10–30 days, the long repeat orbit for C2 requires validation approaches employing some type of spatial and/or temporal averaging.

#### 5.1. Biases

This study reports on the Baseline C version of COP and the issue of the biases between LRM and SAR has been a key focus of the recently implemented Baseline D version. In regions where the operating mode changes, given these biases, any trends or seasonal cycles need to be treated with caution until using the full timeseries from the improved Baseline D dataset. The method described above using successive differences in SSHA, SWH and WSP did not conclusively identify any consistent bias most likely due to a limited number of valid observations. This is also the case for the operational monthly reports that considers pairs of points (closest SAR location to matching LRM point) that finds good agreement.

For SSHA, WSP and SWH there are seasonally varying biases between data from ascending passes versus descending passes, although much less substantive in SWH (overlaps with zero; Fig. 7). In fact, these biases vary by hemisphere. For SSHA, the bias tends to be positive in the Northern Hemisphere (i.e. ascending greater than descending) whereas the opposite is the case in the Southern Hemisphere. Predominantly the finding for the global SSHA bias is negative; supporting the finding of Fig. 4 that descending passes provide higher SSHA compared to ascending passes (influence of Southern Hemisphere higher due to more data). The bias in WSP is somewhere between the other variables with strong seasonal cycles but notable biases especially for the Southern Hemisphere towards the end of the timeseries. In combination with Fig. 4c, there is some evidence that WSP from descending passes are higher than WSP from ascending passes.

Naeije et al. (2023) contains further discussion of these biases, but in summary they calculated that between SAR mode and LRM for SSHA a 1.4 cm difference in range bias exists. This is explained by a 0.5 cm *jump* in sea state bias (corresponding to an equivalent SWH jump of 10.5 cm) the remaining 0.9 cm is due to a range bias between ascending and descending passes relating to a timing bias of 0.367 ms. In addition, Naeije et al. noted issues with the ionosphere and pole tide correction with the latter giving rise to an east—west pattern in range bias.

#### 5.2. SSHA

#### 5.2.1. Global and regional SSHA trends

Globally the trend in LRM SSHA from C2 is  $4.2 \pm 0.3$  mm/year (trend based on OLS with standard error of trend, accounting for serial correlation). This value is in agreement with results from the reference missions (Fig. 4a) although is marginally lower than the values from Colorado ( $4.5 \pm 0.1$  mm/year) and Beckley ( $4.3 \pm 0.1$  mm year/year). Similarly there is no significant difference between GMSL based on ascending passes ( $4.3 \pm 0.3$  mm/year) and GMSL from descending passes ( $4.2 \pm 0.2$  mm/year).

In general, the regional trends in LRM SSHA are positive (Fig. 5a) except for a few regions but these are in agreement with other studies. Due to a known offset in SSHA between LRM and SAR there a number of regions for which no SSHA trend has been calculated, notably Pacific SAR box (Fig. 1) and Northwest European Shelf.

## 5.2.2. PSMSL

In this study we used mean, gridded SSHA from C2 and compared, via correlations, to a set of high-quality tide gauges from the PSMSL. A variety of grid sizes were tested (from 0.5° to 10°), but the optimal balance of representativity and number of observations was found to be 1°. For all tide gauges, the significant correlations were positive with a mean of 0.67 for LRM and 0.59 for SAR. The number of cells with tides gauges that can be paired with SAR data is much less than the number with LRM data (17 cf 65). There are a number of locations that correspond to both LRM and SAR data and these show similar relationships of the tide gauges (inset of Fig. 8a). The correlations of C2 and tide gauges here are similar, albeit slightly lower, to other studies (e.g. Benveniste et al., 2020; Naeije et al., 2023). This is perhaps not surprising as C2 data in this study take no account of the proximity of the altimetry measurements to the tide gauge within the grid cell, unlike the higher correlations found in Naeije et al. (2023).

The geographical distribution of the PSMSL dataset matching all quality control constraints is far from ideal with a predominance in the Northern Hemisphere with the notable exception of parts of the Australian coast. The number of tide gauges is a function of the latency of the tide gauge data, as such repeating the analysis at a later stage might result in incorporating more tide gauge locations. Similarly, using less stringent quality control criteria or allowing shorter time scales would also increase the number of locations. However, these would also have impacts on the correlations. Less stringent selection criteria are routinely used in the monthly reports.

#### 5.3. SWH

For SWH there are no significant values in global trends either overall, based only on ascending passes or based only on descending passes (Fig. 4b; all  $0.0 \pm 0.0$  m/year). Except in the Indian Ocean, the regional pattern in SWH trends (Fig. 5b) is in agreement with Young and Ribal (2019). The visibility of tracks (*trackiness*) in Fig. 5b suggests that the results are perhaps being influenced by individual storms and, at least on a regional basis, longer timeseries would be preferable.

The monthly quality reports provide comparisons of SWH from C2 compared to that from the WW3 model. On average WW3 has a mean ~15 cm above C2 (based on monthly reports 2021–2023) with a few exceptions. In this study, we have considered WW3 and C2 SWH on the same monthly, 2.5° grid. Over most of the time series (Fig. 9a), we found that gridded C2 SWH minus WW3

SWH was about -10 to -20 cm (i.e. same magnitude as that found in the monthly reports). We are not sure why the period mid-2012 to early 2015 does not match, it may be related to fewer LRM data. The global correlation between gridded SWH from C2 and WW3 are consistent varying with the seasonal cycle between 0.8 and 0.9 (Fig. 9b) and there are no anomalous values in the correlation during mid-2012 to early-2015.

The difference between gridded C2 SWH and WW3 is markedly different between hemisphere: the bias is greater in the Southern Hemisphere. However, the variability of the correlation is much more variable in the Northern Hemisphere with two troughs in most years including dropping as low as 0.6 in 2023 compared to the peak values of  $\sim 0.9$ . The Southern Hemisphere correlation is  $\sim 0.85$  and only varies by about 0.05.

The pattern in gridded mean SWH from C2 as a function of gridded mean SWH from C2 minus WW3 suggests there is no clear difference in hemisphere (Fig. 10). However, there is a consistent pattern in the relationship that at low SWH there is a small, negative bias (WW3 tends to be higher than C2), whereas at higher SWH the opposite is the case with C2 SWH higher than WW3. Given the opposite result was identified for a previous processor chain in Calafat et al. (2017) when results were considered monthly, careful study needs to be undertaken in studies of Baseline D. This is especially true given that Fig. 11 might contradict the findings on the sign of the bias from Fig. 10, although interpretation of Fig. 10 is limited by the logarithmic colour scale. The individual monthly differences (supp info) support the finding that the variability of differences is highly variable with large areas with positive differences. Further studies on SWH are limited by the geographical location of wave buoys with most buoys located in the Northern Hemisphere. The hemispheric differences at higher SWH/latitudes might be related to more observations (i.e. ocean area) in the Southern Hemisphere.

## 5.4. WSP

The trend in global WSP is  $3.3 \pm 0.2$  (cm/s)/year with the trends from ascending passes and descending passes in agreement within uncertainties. For most, but not all, months the mean WSP from descending passes is higher than that from ascending passes. It should be remembered that satellite altimeters are unable to measure at low values of WSP and as such care must be taken in comparing these values with other models or datasets.

Regionally, apart from a few, small areas, the trends in WSP from C2 are positive (Fig. 5c) and agree with Young and Ribal (2019). The exception is the negative trends seen in Young and Ribal centred around Southeast Asia are not clear in the C2 data. Although not as obvious as for SWH, there is some *trackiness* again suggesting use of reduced spatial resolution or longer timeseries. The pattern in trends in WSP from C2 compared to ERA5 suggest further

work is required on this relationship. However, this is complicated by C2 not resolving low WSP.

Comparisons of the values of gridded C2 WSP as a function of the bias between C2 and ERA5 WSP are also complicated by C2 not showing the full distribution of C2 WSP. As C2 WSP increases so does the negative bias (i.e. ERA5 WSP is higher than C2 WSP). Conversely, as C2 WSP decreases the opposite is the case (i.e. C2 WSP is higher than ERA5).

#### 6. Conclusion

In this study we have demonstrated the quality and consistency of the C2 Baseline C GOP over a 13-year period for SSHA, SWH and WSP. An improved processing chain (Baseline D) has recently been introduced (October 2024) and a future study will aim to repeat a similar long-term review of the quality of this new product. The performance is already being monitored through the daily and monthly reports discussed in Section 2 above. It is worth noting that the routine reports not only provide information on GOP but also on the quality and performance of the TC products (NOP and IOP).

Apart from the bias observed between LRM and SAR mode for SSHA, the quality of SSHA data from C2 are excellent. Over the study period, C2 has measured an increase of GMSL of about 5.5 cm comparable to the values of 5.9 cm and 5.6 cm from Colorado and Beckley respectively. Many dynamic regions (e.g. Kuroshio and Agulhas) are omitted from the C2 assessment of GMSL as they are primarily covered by SAR mode; reduced or zero bias between SSHA from SAR mode and LRM in Baseline D will enable GMSL to be calculated to include these regions.

What is perhaps surprising in the global trends is that although C2 suggests an increase in global mean wind speed of about 0.4 m/s over the study period, there is no change in SWH. The reasons for this are not obvious and may be in some way related to C2 unable to measure low wind speeds. Young and Ribal (2019) found evidence that changes in the 90th percentile for both SWH and WSP are increasing faster than the trends in the means. In addition, they observed significant trends over a greater area for WSP compared with SWH.

The results of the validation against tide gauge observations confirms that the values of SSHA from C2 in the coastal zone are comparable in quality to measurements from other satellites. In particular, we find an average correlation of 0.67 for LRM and 0.59 for SAR over all the tide gauges for monthly values, which is higher than the average correlation of 0.5 reported for along-track data from the Jason satellite series derived using dedicated coastal retracking (Benveniste et al., 2020; Cazenave et al., 2022). The correlation that we find for C2 (0.67 for LRM) is slightly lower than the values found for multi-mission gridded altimetry products, such as the one from the Copernicus Marine Environment Monitoring Service, which are

typically > 0.7 (Benveniste et al., 2020). However, this is to be expected because such gridded products are generated using more sophisticated gridding algorithms that minimise the effects of small-scale variability and measurement errors, leading to higher correlations with tide gauge data.

Potentially contradictory information on differences between SWH from C2 and model output (WW3) should be investigated further perhaps using additional data (e.g. from buoys). For example, we have found that at high latitudes, especially in the Southern Ocean, C2 tends to show lower values of SWH than WW3. Past studies have found similar biases when comparing observations from Jason-1 with data from WW3 (Ardhuin et al., 2010), which suggests that the issue is with WW3 rather than C2. This is further supported by the good agreement between buoys and SWH from C2 as shown in the monthly reports, although in this case one should consider the limited geographical position of the selected buoys (i.e. focussed around the coast of North America) and that any further study should consider incorporating a wider selection of locations.

## **Declaration of competing interest**

The authors declare that they have no known competing financial interests or personal relationships that could have appeared to influence the work reported in this paper.

#### Acknowledgements

This work was funded by the European Space Agency under the CryOcean-QCV project (contract 4000132722). The authors are grateful to the numerous colleagues who have contributed to CryOcean-QCV over the last 11 years through provision of data, contributions to code, suggestions for changes and helpful conversations. Special thanks to Dr Stefano Vignudelli (Associate Editor) and the two anonymous reviewers for their constructive input in improving this manuscript.

## Appendix A. Supplementary material

Supplementary material to this article can be found online at https://doi.org/10.1016/j.asr.2025.06.051.

#### References

- Andersen, O.B., 2010. The DTU10 gravity field and mean sea surface. Second International Symposium of the Gravity Field of the Earth (IGFS2). Fairbanks, Alaska, USA.
- Andersen, O.B., 2022. DTU21 Mean Sea Surface. DTU https://doi.org/ 10.11583/DTU.19383221.
- Andersen, O.B., Knudsen, P., 2009. DNSC08 mean sea surface and mean dynamic topography models. J. Geophys. Res. Oceans 114.
- Ardhuin, F., Rogers, E., Babanin, A.V., et al., 2010. Semiempirical dissipation source functions for ocean waves. Part I: Definition, calibration, and validation. J. Phys. Oceanogr. 40, 1917–1941.

- Banks, C.J., Calafat, F.M., Shaw, A.G.P., Snaith, H.M., Gommenginger, C.P., Bouffard, J., 2023. A new daily quarter degree sea level anomaly product from CryoSat-2 for ocean science and applications. Sci. Data 10, 477.
- Beckley, B., Yang, X., Zelensky, N.P., et al., 2021. Global Mean Sea Level Trend from Integrated Multi-Mission Ocean Altimeters TOPEX/Poseidon, Jason-1, OSTM/Jason-2, and Jason-3 Version 5.1, 5.1 ed. PO.DAAC, CA, USA.
- Beckley, B.D., Callahan, P.S., Hancock III, D.W., Mitchum, G.T., Ray, R.D., 2017. On the "Cal-Mode" correction to TOPEX satellite altimetry and its effect on the global mean sea level time series. J. Geophys. Res. Oceans 122, 8371–8384.
- Benveniste, J., Birol, F., Calafat, F., et al., 2020. Coastal sea level anomalies and associated trends from Jason satellite altimetry over 2002–2018. Sci. Data 7, 357.
- Benveniste, J., Cazenave, A., Vignudelli, S., et al., 2019. Requirements for a coastal hazards observing system. Front. Mar. Sci. 6, 24.
- Bouffard, J., Naeije, M., Banks, C.J., et al., 2018. CryoSat ocean product quality status and future evolution. Adv. Space Res. 62, 1549–1563.
- Calafat, F.M., Cipollini, P., Bouffard, J., Snaith, H., Féménias, P., 2017.
  Evaluation of new CryoSat-2 products over the ocean. Remote Sens.
  Environ. 191, 131–144.
- Cazenave, A., Gouzenes, Y., Birol, F., et al., 2022. Sea level along the world's coastlines can be measured by a network of virtual altimetry stations. Commun. Earth Environ. 3, 117.
- Cheung, K.F., 2010. WaveWatch III (WW3) Global Wave Model. Pacific Islands Ocean Observing System (PacIOOS) (updated 2021).
- Chib, S., 1993. Bayes regression with autoregressive errors: a Gibbs sampling approach. J. Econ. 58, 275–294.
- Donlon, C.J., Cullen, R., Giulicchi, L., et al., 2021. The Copernicus sentinel-6 mission: Enhanced continuity of satellite sea level measurements from space. Remote Sens. Environ. 258 112395.
- European Space Agency, 2019. Baseline-C CryoSat Ocean Processor: Ocean Product Handbook. Frascati, Italy.
- Fenoglio, L., Dinardo, S., Uebbing, B., et al., 2021. Advances in NE-Atlantic coastal sea level change monitoring by Delay Doppler altimetry. Adv. Space Res. 68, 571–592.
- Fernandes, M.J., Lazaro, C., 2016. GPD plus wet tropospheric corrections for CryoSat-2 and GFO altimetry missions. Remote Sens. (Basel) 8.
- Hersbach, H., Bell, B., Berrisford, P., et al., 1940. ERA5 monthly averaged data on single levels from 1940 to present. Copernicus Climate Change Service (C3S) Climate Data Store (CDS).
- Holgate, S.J., Matthews, A., Woodworth, P.L., et al., 2013. New data systems and products at the permanent service for mean sea level. J. Coast. Res. 29, 493–504.
- Kalnay, E., Kanamitsu, M., Kistler, R., et al., 1996. The NCEP/NCAR 40-year reanalysis project. Bull. Am. Meteorol. Soc. 77, 437–472.
- Legeais, J.F., Ablain, M., Zawadzki, L., et al., 2018. An improved and homogeneous altimeter sea level record from the ESA climate change initiative. Earth Syst. Sci. Data 10, 281–301.
- Naeije, M., Bouffard, J., 2021. Long-term quality and stability assessment of CryoSat-2 ocean data. Adv. Space Res. 68, 1194–1215.
- Naeije, M., Di Bella, A., Geminale, T., Visser, P., 2023. CryoSat long-term ocean data analysis and validation: Final words on GOP baseline-C. Remote Sens. (Basel) 15.
- Parrinello, T., Shepherd, A., Bouffard, J., et al., 2018. CryoSat: ESA's ice mission Eight years in space. Adv. Space Res. 62, 1178–1190.
- Passaro, M., Cipollini, P., Vignudelli, S., Quartly, G.D., Snaith, H.M., 2014. ALES: A multi-mission adaptive subwaveform retracker for coastal and open ocean altimetry. Remote Sens. Environ. 145, 173– 180
- Permanent Service for Mean Sea Level (PSMSL), 2023. Tide Gauge Data. In: Centre, N.O., (Ed.).
- Sea Level Research Group, University of Colorado. 2023\_rel2: Global Mean Sea Level (Seasonal Signals Retained). 2023.

- The MathWorks Inc., 2020. MATLAB Version: 9.9.0.2037887 (R2020b) Update 8. The MathWorks Inc, Natick, Massachusetts, United States.
- Tran, N., 2015. Envisat Phase-F: Sea State Bias. Technical Report CLS-DOS-NT-15-031, ESA contract "ENVISAT RA-2 AND MWR ESL and Prototypes Maintenance Support (Level 1B and Level 2).
- Vignudelli, S., Birol, F., Benveniste, J., et al., 2019. Satellite altimetry measurements of sea level in the coastal zone. Surv. Geophys. 40, 1319–1349.
- Young, I.R., Ribal, A., 2019. Multiplatform evaluation of global trends in wind speed and wave height. Science 364, 548–552.